Bond distortion effects and electric orders in spiral multiferroic magnets

2013 J. Phys.: Condens. Matter 25 286004

(http://iopscience.iop.org/0953-8984/25/28/286004)

J. Phys.: Condens. Matter **25** (2013) 286004 (14pp) doi:10.1088/0953-8984/25/28/286004

Bond distortion effects and electric orders in spiral multiferroic magnets

Hong-Bo Chen, Yi Zhou and You-Quan Li

Zhejiang Institute of Modern Physics and Department of Physics, Zhejiang University, Hangzhou 310027, People's Republic of China

E-mail: hbchen@zju.edu.cn

Received 24 February 2013
Published 19 June 2013
Online at stacks.iop.org/JPhysCM/25/286004

Abstract

In this paper we study the bond distortion effect on the electric polarization in spiral multiferroic magnets based on cluster and chain models. The bond distortion breaks the inversion symmetry and modifies the d–p hybridization. Consequently, it will affect the electric polarization, which can be divided into the spin-current part and the lattice-mediated part. The spin-current polarization can be written in terms of $\vec{e}_{i,j} \times (\vec{e}_i \times \vec{e}_j)$ with anisotropic amplitude, and the lattice-mediated polarization exists only when the M–O–M bond is distorted. The electric polarization for three-atom M–O–M and four-atom M–O_2–M clusters is calculated. We also study possible electric ordering in three kinds of chains made of different clusters. We apply our theory to multiferroic cuprates and find that the results are qualitatively in agreement with experimental observations.

(Some figures may appear in colour only in the online journal)

1. Introduction

Magnetoelectric multiferroics, where magnetic and electric ordering coexist in a single compound, have attracted much interest in the last few decades due to their potential for novel physics and technological applications [1]. However, the initial observations have shown that materials with coexisting ferroelectric and magnetic orders are rare in nature and the observed magnetoelectric coupling was rather weak [2]. Therefore, the search for new gigantic magnetoelectric multiferroic materials is a great challenge. Important progress in multiferroics was made by Kimura *et al* [3] who found giant magnetoelectric effects in the perovskite manganite $TbMnO_3$ in 2003. The ferroelectric transition at $T_c = 28$ K in $TbMnO_3$ was ascribed to the emergence of a nontrivial magnetic order, i.e., with a spiral spin structure [4]. This finding revived interest in multiferroic behavior and led to the discovery of a relatively large number of spin-driven multiferroic materials [5–8].

One of the fundamental issues in multiferroic physics is to clarify the origin of the magnetoelectric coupling in such new materials. Currently, although several models have been proposed both microscopically [9–18] and phenomenologically [19], the microscopic mechanism of the magnetoelectric coupling is still a controversial and unresolved topic. One of the most prevailing mechanisms is the spin-current model proposed by Katsura *et al* [9] for helical magnets. They studied a three-atom M–O–M (M denotes a transition metal ion and O is for an oxygen ion) cluster where O locates in the inversion center of the cluster, say, the mid-point between two M ions. They pointed out that spontaneous electric polarization in the spiral magnetic order arises from a distortion of electronic density even without ionic or atomic displacements. And the polarization can be expressed in the form

$$\vec{P} \propto \vec{e}_{i,j} \times (\vec{e}_i \times \vec{e}_j), \tag{1}$$

where $\vec{e}_{i,j}$ denotes the bond direction connecting the two neighbor spin moments $\vec{S}_i$ and $\vec{S}_j$ along directions $\vec{e}_i$ and $\vec{e}_j$ on the sites i and j respectively. The electric polarization is closely associated with the nonzero spin current $\vec{S}_i \times \vec{S}_j$ between two neighboring noncollinear spins. Furthermore, Jia *et al* [10, 11] presented a more sophisticated calculation on the spin-current model with realistic considerations. Their results showed that the spin-current model is able to explain many experimental data at least semiquantitatively. On the other hand, Sergienko and Dagotto [16] argued that the ferroelectric polarization is closely related to the inverse Dzyaloshinskii–Moriya (DM) coupling which breaks inversion symmetry and obtained a similar expression for

electric polarization as in (1). Interestingly, the spin–orbit interaction plays a crucial role in both theories. The role of spin–orbit interaction was also confirmed by Mostovoy based on the phenomenological theory [19]. Experimentally, the spin-current mechanism was demonstrated directly by controlling the spin-helicity vector in $TbMnO_3$ with an external electric field [20]. The spin-current mechanism has also been applied to several other spiral multiferroic materials, such as $DyMnO_3$ [21], $MnWO_4$ [22], $Ni_3V_2O_8$ [23], $CoCr_2O_4$ [24], $LiCu_2O_2$ [25, 26] and $LiCuVO_4$ [27–30]. Besides these successful applications, it should be noted that the magnitude of electric polarization is very sensitive to the location of Fermi energy in existing spin-current models. When the Fermi energy locates between two hybridized levels, which refers to the 'single hole' in [9], $P \propto V/\Delta$, where V is the hybridization between transition metal d-orbitals and oxygen p-orbitals and Δ is the energy difference between d-orbitals and p-orbitals. Whereas, when the Fermi energy locates outside two hybridized levels, which refers to the 'double hole' in [9], $P \propto (V/\Delta)^3$, which is significantly different from the 'single-hole' situation. Recently, Xiang *et al* [31] have also developed a generalized spin-current model for multiferroicity in a helical magnetic structure and have applied the theory to a variety of novel multiferroics, such as MnI_2 [31], $CaMn_7O_{12}$ [32], Cu_2OSeO_3 [33] and $Cu_3Nb_2O_8$ [34].

In real multiferroics, their fascinating properties are attributed to the competition among charge, spin, orbital, and lattice degrees of freedom. Actually, the bond distortion is inevitably present in realistic transition metal oxides due to structure distortion [35, 36]. Thus, the inversion symmetry breaks and the oxygen atom is away from the mid-point between two M atoms. Therefore, the bond distortion effects should be taken into account in the calculation for the electric polarization. In existing spin-current model [9–11], the bond distortion effect is overlooked. As a result, which we shall show in this paper, the calculated electric polarization is underestimated. A recent theoretical study on a toy model for the ferroelectricity of a two-dimensional cluster [14] suggests that the bond-bending may be important for the enhancement of the ferroelectricity due to orbital hybridization. On the other hand, Moskvin *et al* [37] argued that the cluster model in [9] is oversimplified to account for $LiCu_2O_2$ and $LiCuVO_4$ in which the realistic geometry configuration of the oxygen atoms was not considered. All of these facts motivate the present work to explore the effect of bond distortion on the electric polarization in the spiral multiferroic magnets in the framework of the spin-current model.

The organization of this paper is as follows. In section 2, we perform quantum chemistry analysis on relevant d-orbitals and construct cluster models with two M atoms and bridge oxygen atoms. Then we calculate lowest lying eigenstates for these cluster models. In section 3, we calculate the electric polarization for different clusters. In section 4, we discuss three kinds of chain models formed by different clusters and possible ordering of electric polarization. In section 5, we discuss the relation between lattice-driven polarization and magnetic-driven polarization and apply our theory to multiferroic copper oxides. Section 6 is devoted to the summary.

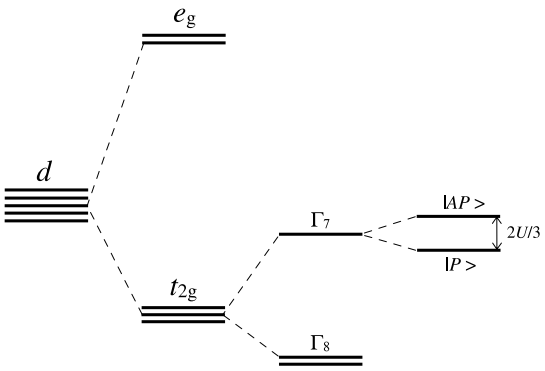

Figure 1. Relevant electronic states at transition metal atoms. Five-fold degenerate d-orbitals will split into two fold e_g and three-fold t_{2g} levels. The spin–orbit interaction λ splits t_{2g} levels to a doublet Γ_7 and a quartet Γ_8. In the presence of effective exchange U between Γ_7 electrons and local magnetic moment, Γ_7 will be further split into spin parallel state $|P\rangle$ and anti-parallel state $|AP\rangle$. It is worth noting that the order of energy levels will reverse as we take the hole picture in the following.

2. Cluster models

We begin with quantum chemistry consideration. As is well known, when the 3d transition metal atoms are placed in an octahedral crystal field, the five-fold degenerate d levels will split into e_g and t_{2g} levels. Incorporating the on-site spin–orbit interaction λ, the e_g orbitals will not be influenced but the t_{2g} manifold will further split into a doublet Γ_7 and a quartet Γ_8 (see figure 1). For simplicity and following Katsura *et al* [9], we will adopt the following Γ_7 states as the ground state manifold and drop the quartet,

$$\begin{aligned} |a\rangle &= \frac{1}{\sqrt{3}}\left(\left|\mathrm{d}_{xy,\uparrow}\right\rangle + \left|\mathrm{d}_{yz,\downarrow}\right\rangle + \mathrm{i}\left|\mathrm{d}_{zx,\downarrow}\right\rangle\right), \\ |b\rangle &= \frac{1}{\sqrt{3}}\left(\left|\mathrm{d}_{xy,\downarrow}\right\rangle - \left|\mathrm{d}_{yz,\uparrow}\right\rangle + \mathrm{i}\left|\mathrm{d}_{zx,\uparrow}\right\rangle\right), \end{aligned} \tag{2}$$

by assuming the spin–orbit coupling λ is the largest energy scale of the problem.

As in [9], we further invoke the effective exchange interaction between Γ_7 electrons and local magnetic moment governed by the following Hamiltonian,

$$H_U = -U\sum_j \vec{e}_j \cdot \vec{S}_j, \tag{3}$$

where $\vec{e}_j = (\cos\phi_j \sin\theta_j, \sin\phi_j \sin\theta_j, \cos\theta_j)$ is the unit vector of the local magnetic moment from the transition metal atom M at jth site, $\vec{S}_j$ the total spin operator of the d-orbital electrons, U the effective exchange interaction which is of the order of Coulomb interaction and Hund's coupling energy [9–11]. Then H_U will further split the Γ_7 doublet into spin parallel state $|P\rangle$ and anti-parallel state $|AP\rangle$,

$$\left|P_j\right\rangle = \sin\frac{\theta_j}{2}\left|a\right\rangle + \mathrm{e}^{\mathrm{i}\phi_j}\cos\frac{\theta_j}{2}\left|b\right\rangle, \tag{4a}$$

$$\left|AP_j\right\rangle = \cos\frac{\theta_j}{2}\left|a\right\rangle - \mathrm{e}^{\mathrm{i}\phi_j}\sin\frac{\theta_j}{2}\left|b\right\rangle, \tag{4b}$$

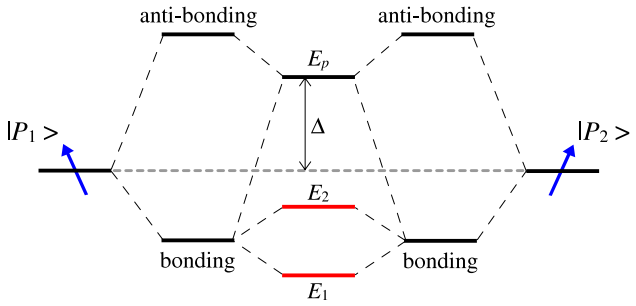

Figure 2. Energy levels demonstration for a M–O–M cluster.

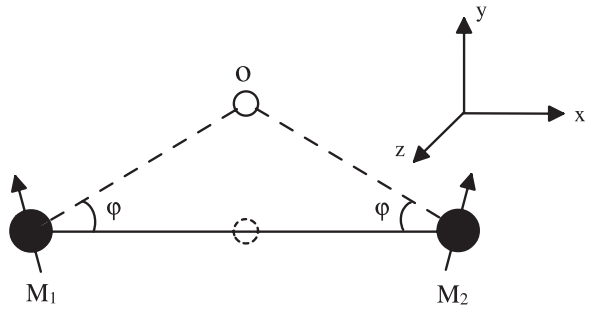

Figure 3. The three-atom M–O–M cluster model. M_1 and M_2 denote two transition metal ions with noncollinear magnetic moments. O represents a bridge oxygen atom which deviates from its centrosymmetric position (denoted by the dash circle) with a bond-bending angle φ. The arrows on M_1 and M_2 indicate the spin direction. The three atoms of the cluster are assumed to be lying in the *xy* plane.

where $|P_j\rangle$ and $|AP_j\rangle$ indicate the spin state parallel and anti-parallel to the unit vector $\vec{e}_j$, and the corresponding eigenvalues are $E_{|P_j\rangle} = -\frac{U}{3}$ and $E_{|AP_j\rangle} = \frac{U}{3}$, respectively. Note that we may further write $|P_j\rangle$ and $|AP_j\rangle$ in terms of t_{2g} states,

$$|P_j\rangle = \sum_{\mu\sigma} A_{(j)}^{\mu\sigma} |d_{\mu\sigma}^{(j)}\rangle, \tag{5a}$$

and

$$|AP_j\rangle = \sum_{\mu\sigma} B_{(j)}^{\mu\sigma} |d_{\mu\sigma}^{(j)}\rangle, \tag{5b}$$

where $\mu = xy, yz, zx, \sigma = \uparrow, \downarrow$, $A_{(j)}^{\mu\sigma}$ and $B_{(j)}^{\mu\sigma}$ are coefficients obtained from combining equations (4*a*) and (4*b*) and (2) which depend on angles θ_j and ϕ_j (see appendix A for details). Hereafter, we assume that λ and U are much larger than other relevant energy scales so that there is only one relevant state in each M atoms, say, $|P\rangle$. We also assume that there is a spiral magnetic order relating to the transition metal atoms.

Now we are in the position to construct cluster models by including bridge oxygen atoms between two M atoms. Taking the hole picture, we assume that the oxygen p-orbital has energy level E_p which is above $E_{|P\rangle}$ with a difference Δ as shown in figure 2, i.e. $E_p = E_{|P\rangle} + \Delta$. The hybridization between spin parallel state $|P\rangle$ and oxygen p-orbitals results in bonding and anti-bonding states with lower and higher energy, respectively. In such a M–O–M cluster (see figure 2), left and right bonding states will further hybridize with each other and lead to two lowest energy levels E_1 and E_2. When the Fermi energy E_F locates between E_1 and E_2, it is called the 'single hole' in [9]. It is called the 'double hole' when E_F is above E_2 but below other levels.

The hybridization between left and right bonding states will also lead to distorted electronic density and thereby possible electric polarization in such a M–O–M cluster. We may further consider more bridge oxygen atoms between two M atoms and derive similar electronic density distortion and electric polarization. We shall study a three-atom M–O–M cluster and a four-atom M–O_2–M cluster in the remaining part of this section and calculate electric polarization for different kinds of chains formed by three-atom or four-atom clusters in section 2.1.

2.1. Three-atom M–O–M cluster

Firstly we consider the three-atom M–O–M cluster model shown in figure 3. M_1 and M_2 refer to two transition metal atoms and the intermediate oxygen atom (O) deviates from its centrosymmetric position on the M_1–M_2 bond. Simply, we assume that the three atoms of the cluster are restricted within the *xy*-plane, the M_1–M_2 bond is along the *x*-axis, and the lengths of two M–O bonds are equal to each other. Note that Katsura *et al* [9] considered a centrosymmetric three-atom model in which the oxygen atom locates at the mid-point between two M atoms.

Upon the above quantum chemistry analysis, we use the following Hamiltonian to describe the on-site energy for oxygen p-orbitals and spin parallel states,

$$H_\Delta = \sum_{j=1,2} E_{|P\rangle} c_{|P_j\rangle}^\dagger c_{|P_j\rangle} + \sum_{\mu,\sigma} (E_{|P\rangle} + \Delta) p_{\mu,\sigma}^\dagger p_{\mu,\sigma}, \tag{6}$$

where $p_{\mu,\sigma}, (\mu = x, y, z)$ are annihilation operators for oxygen p-electrons, σ is the spin index, $c_{|P_j\rangle}$ is the annihilation operator for spin parallel state at site *j*.

The hybridization between p-orbitals and spin parallel states is governed by the hopping Hamiltonian,

$$H_t = H_t^{1-m} + H_t^{2-m} + \text{H.c.}, \tag{7}$$

where H_t^{1-m} and H_t^{2-m} indicate the hopping processes between the oxygen atom and M_1 and M_2 respectively. We then write down H_t^{1-m} and H_t^{2-m} in terms of nonvanishing hopping integrals explicitly,

$$H_t^{1-m} = \sum_\sigma \Big(V_1 p_{x,\sigma}^\dagger d_{xy,\sigma}^{(1)} + V_2 p_{y,\sigma}^\dagger d_{xy,\sigma}^{(1)} + V_3 p_{z,\sigma}^\dagger d_{zx,\sigma}^{(1)} + V_4 p_{z,\sigma}^\dagger d_{yz,\sigma}^{(1)} \Big), \tag{8}$$

$$H_t^{2-m} = \sum_\sigma \Big(V_1 p_{x,\sigma}^\dagger d_{xy,\sigma}^{(2)} - V_2 p_{y,\sigma}^\dagger d_{xy,\sigma}^{(2)} - V_3 p_{z,\sigma}^\dagger d_{zx,\sigma}^{(2)} + V_4 p_{z,\sigma}^\dagger d_{yz,\sigma}^{(2)} \Big), \tag{9}$$

where $d_{\mu,\sigma}^{(j)}$ $(\mu = xy, yz, zx)$ are annihilation operators for d electrons of the transition metal atoms. The superscript $j = 1, 2$ in $d_{\mu,\sigma}^{(j)}$ denote the site of magnetic transition metal atoms as shown in figure 3. The integrals V_n $(n = 1, 2, 3, 4)$ between d- and p-orbitals are given according to

Slater–Koster's rules [38] as follows,

$$\begin{aligned} V_1 &= \sin\varphi\left(\sqrt{3}\cos^2\varphi t_{\mathrm{pd}\sigma} + (1-2\cos^2\varphi)t_{\mathrm{pd}\pi}\right), \\ V_2 &= \cos\varphi\left(\sqrt{3}\sin^2\varphi t_{\mathrm{pd}\sigma} + (1-2\sin^2\varphi)t_{\mathrm{pd}\pi}\right), \\ V_3 &= \cos\varphi t_{\mathrm{pd}\pi}, \\ V_4 &= \sin\varphi t_{\mathrm{pd}\pi}. \end{aligned} \tag{10}$$

Here φ is the angle between M_1–M_2 bond (i.e., along x-axis) and $M_{1(2)}$–O bond, as shown in figure 3. $t_{\mathrm{pd}\sigma}$ and $t_{\mathrm{pd}\pi}$ are hybridization integrals corresponding to σ and π bonding between p- and d-orbitals, respectively. In contrast to the hopping Hamiltonian derived by Katsura *et al* in [9] where only $t_{\mathrm{pd}\pi}$ is present due to inversion symmetry, there are four relevant and independent hopping integrals V_n, $n = 1, 2, 3, 4$. More active orbitals are involved in our model due to the bond distortion, such as p_x and d_{yz} orbitals. Thus, the Hilbert space in the present model is enlarged. The basis of the our cluster system contains $|P_j\rangle$, $(j = 1, 2)$ and $p_{\mu,\sigma}$ $(\mu = x, y, z,\ \sigma = \uparrow, \downarrow)$ and an eigenstate is a linear combination of these states. We can easily recover the centrosymmetric cluster model in [9] by setting $\varphi = 0$, which leads to $V_1 = V_4 = 0$ and $V_2 = V_3$.

We proceed to calculate the eigenstates of the system by assuming $V \ll \Delta$ and treating H_t as a perturbation to H_Δ. To the second order perturbation [39], the two lowest lying states are given by energy levels

$$E_{1(2)} = 2(C \mp |B|), \tag{11}$$

with corresponding eigenvectors $|1\rangle$ and $|2\rangle$ given in appendix B, where the parameters C and B are as follows,

$$\begin{aligned} C &= -\frac{V_1^2 + V_2^2 + V_3^2 + V_4^2}{3\Delta}, \\ B &= A_1\alpha + A_2\beta, \end{aligned} \tag{12}$$

with

$$\begin{aligned} A_1 &= -\frac{V_1^2 - V_2^2 - V_3^2 + V_4^2}{3\Delta}, \\ A_2 &= \frac{2V_3V_4}{3\Delta}, \end{aligned} \tag{13}$$

and

$$\begin{aligned} \alpha &= \sin\frac{\theta_1}{2}\sin\frac{\theta_2}{2} + \cos\frac{\theta_1}{2}\cos\frac{\theta_2}{2}\mathrm{e}^{-\mathrm{i}(\phi_1-\phi_2)}, \\ \beta &= \mathrm{i}\left[\sin\frac{\theta_1}{2}\sin\frac{\theta_2}{2} - \cos\frac{\theta_1}{2}\cos\frac{\theta_2}{2}\mathrm{e}^{-\mathrm{i}(\phi_1-\phi_2)}\right]. \end{aligned} \tag{14}$$

The angles (θ_1, ϕ_1) and (θ_2, ϕ_2) specify the direction of local magnetic moments in transition metal atom M_1 and M_2, respectively. For a centrosymmetric cluster with $\varphi = 0$, we have $A_2 = 0$ and $C = -A_1$.

2.2. Four-atom M–O_2–M cluster

Secondly, we consider the four-atom M–O_2–M cluster illustrated in figure 4. In this situation, there are two oxygen atoms symmetrically deviated away from the M_1–M_2 bond with bending angle φ. Here, we also assume that the atoms of the cluster are restricted within the xy plane and the M_1–M_2 bond is along the x-axis for convenience.

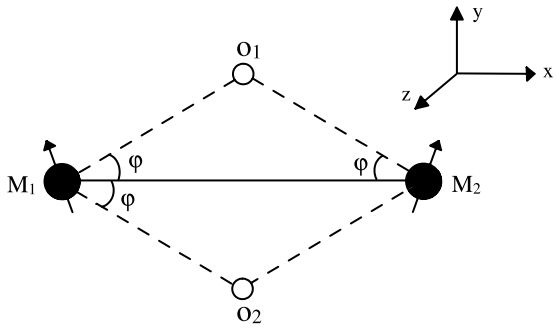

Figure 4. Four-atom M_1–$O_{1(2)}$–M_2 cluster. Two bridge oxygen atoms O_1 and O_2 symmetrically deviates from M_1–M_2 bond with a bond distortion angle φ. The arrows on M_1 and M_2 indicate the directions of spins. The four atoms of this cluster lie within the xy plane and M_1–M_2 bond lies along the x-axis.

The on-site energy in equation (6) is then modified as

$$H_\Delta = \sum_{j=1,2} E_{|P\rangle} c^\dagger_{|P_j\rangle} c_{|P_j\rangle} + \sum_{i,\mu,\sigma} (E_{|P\rangle} + \Delta) \mathrm{p}^{\dagger(i)}_{\mu,\sigma} \mathrm{p}^{(i)}_{\mu,\sigma}, \tag{15}$$

where the superscript $i = 1, 2$ in $\mathrm{p}^{(i)}_{\mu,\sigma}$, $(\mu = x, y, z)$ denotes the site number for oxygen atoms O_1 and O_2 shown in figure 4. Note that we assume that p-orbitals in the two oxygen atoms O_1 and O_2 have the same energy levels, say, $E_{\mathrm{p}_1} = E_{\mathrm{p}_2} = E_{|P\rangle} + \Delta$, due to the symmetric deviation of the two oxygen atoms.

Accordingly, we shall replace hopping terms H_t^{1-m} and H_t^{2-m} in equations (8) and (9) by

$$\begin{aligned} H_t^{1-m} = \sum_\sigma \Big(& V_1 \mathrm{p}^{\dagger(1)}_{x,\sigma} \mathrm{d}^{(1)}_{xy,\sigma} + V_2 \mathrm{p}^{\dagger(1)}_{y,\sigma} \mathrm{d}^{(1)}_{xy,\sigma} + V_3 \mathrm{p}^{\dagger(1)}_{z,\sigma} \mathrm{d}^{(1)}_{zx,\sigma} \\ & + V_4 \mathrm{p}^{\dagger(1)}_{z,\sigma} \mathrm{d}^{(1)}_{yz,\sigma} - V_1 \mathrm{p}^{\dagger(2)}_{x,\sigma} \mathrm{d}^{(1)}_{xy,\sigma} + V_2 \mathrm{p}^{\dagger(2)}_{y,\sigma} \mathrm{d}^{(1)}_{xy,\sigma} \\ & + V_3 \mathrm{p}^{\dagger(2)}_{z,\sigma} \mathrm{d}^{(1)}_{zx,\sigma} - V_4 \mathrm{p}^{\dagger(2)}_{z,\sigma} \mathrm{d}^{(1)}_{yz,\sigma} \Big), \end{aligned} \tag{16}$$

and

$$\begin{aligned} H_t^{2-m} = \sum_\sigma \Big(& V_1 \mathrm{p}^{\dagger(1)}_{x,\sigma} \mathrm{d}^{(2)}_{xy,\sigma} - V_2 \mathrm{p}^{\dagger(1)}_{y,\sigma} \mathrm{d}^{(2)}_{xy,\sigma} - V_3 \mathrm{p}^{\dagger(1)}_{z,\sigma} \mathrm{d}^{(2)}_{zx,\sigma} \\ & + V_4 \mathrm{p}^{\dagger(1)}_{z,\sigma} \mathrm{d}^{(2)}_{yz,\sigma} - V_1 \mathrm{p}^{\dagger(2)}_{x,\sigma} \mathrm{d}^{(2)}_{xy,\sigma} - V_2 \mathrm{p}^{\dagger(2)}_{y,\sigma} \mathrm{d}^{(2)}_{xy,\sigma} \\ & - V_3 \mathrm{p}^{\dagger(2)}_{z,\sigma} \mathrm{d}^{(2)}_{zx,\sigma} - V_4 \mathrm{p}^{\dagger(2)}_{z,\sigma} \mathrm{d}^{(2)}_{yz,\sigma} \Big), \end{aligned} \tag{17}$$

respectively, where V_n $(n = 1, 2, 3, 4)$ are the same hybridization integrals defined in equations (10). As shown in section 2.1, due to the oxygen atoms displacements, there are more active orbitals involved. Relevant states in such a four-atom cluster include $|P_j\rangle$, $|AP_j\rangle$ and $\mathrm{p}^{(i)}_{\mu,\sigma}$, where $i, j = 1, 2$, $\mu = x, y, z$, $\sigma = \uparrow, \downarrow$.

In a similar way to the three-atom cluster, the two lowest lying states of the four-atom cluster can be obtained with energy levels,

$$E_{1(2)} = 2(C \mp |A_1\alpha|), \tag{18}$$

and corresponding eigenvectors $|1\rangle$ and $|2\rangle$ given in appendix C, where the parameters C, A_1 and α are those given in equations (12)–(14).

3. Electric polarization in clusters

We shall calculate electric polarizations $\vec{P} = \langle e\vec{r}\rangle$ for three-atom M–O–M clusters or four-atom M–O_2–M clusters using the states $|1\rangle$ and $|2\rangle$ obtained from cluster models in the previous section. The position of Fermi energy E_F is crucial to determine the expectation value $\vec{P}$, which is given by

$$\vec{P} = n_F(E_1 - E_F)\frac{\langle 1|\, e\vec{r}\,|1\rangle}{\langle 1|1\rangle} + n_F(E_2 - E_F)\frac{\langle 2|\, e\vec{r}\,|2\rangle}{\langle 2|2\rangle}, \quad (19)$$

where $n_F(E) = \frac{1}{1+e^{\beta E}}$ is the Fermi function. At low temperature, one may replace $n_F(E)$ by $\theta(-E)$. In the case of a single hole, say, $E_1 < E_F < E_2$, only the lowest state $|1\rangle$ contributes to electric polarization. While in the double-hole situation, $E_F > E_2$, both state $|1\rangle$ and $|2\rangle$ are active [9].

According to the expression of $|1\rangle$ and $|2\rangle$ given in appendices B and C, the electric polarization $\vec{P}$ can be written in terms of the overlap dipole matrix elements $I^{\alpha}_{\mu,\nu}(\vec{a})$ given as follows,

$$I^{\alpha}_{\mu,\nu}(\vec{a}) = e\left\langle \mathrm{d}_{\mu}(\vec{r})\right|\alpha\left|\mathrm{p}_{\nu}(\vec{r}+\vec{a})\right\rangle, \quad (20)$$

where $\vec{a}$ is the displacement from a transition metal atom M to one of its neighboring oxygen atoms O, $\alpha = x, y, z$ is one of the three components of $\vec{r}$, $\mu = xy, yz, zx$ denotes three t_{2g} orbitals and $\nu = x, y, z$ denotes three oxygen p-orbitals. We calculate $I^{\alpha}_{\mu,\nu}(\vec{a})$ in appendix D and study the configurations of electric polarization in the following subsections.

We find that the electric polarization consists of two parts. The first part can be written in terms of $\vec{e}_j \times \vec{e}_{j+1}$, which is called 'spin-current polarization'. The second part depends on the bond-bending angle and distortion configuration, which is called 'lattice-mediated polarization'.

3.1. Three-atom M–O–M cluster

For a three-atom M–O–M cluster, both spin-current polarization and lattice-mediated polarization contribute to the electric polarization. However, they may play different roles in different situations. We shall discuss the single-hole and double-hole situations, respectively.

For the *single-hole situation* when $E_1 < E_F < E_2$, only the lowest state $|1\rangle$ contributes to electric polarization. The induced electric polarization $\vec{P}_{j,j+1}$ at each element cluster connecting j and $j+1$th transition metal atoms can be calculated with the help of equation (B.1). The resulting polarization with three components reads,

$$\begin{aligned}
P^x_{j,j+1} &= 0,\\
P^y_{j,j+1} &= \frac{1}{3}\frac{I^y_1 A_1 + I^y_2 A_2}{\Delta\left|B_{j,j+1}\right|}\left(\vec{e}_{j,j+1}\times(\vec{e}_j\times\vec{e}_{j+1})\right)\big|_y - \frac{2}{3}\frac{I^y_3}{\Delta}\\
&\quad - \frac{2}{3}\frac{I^y_2 A_1\left|\alpha_{j,j+1}\right|^2 + I^y_1 A_2\left|\beta_{j,j+1}\right|^2}{\Delta\left|B_{j,j+1}\right|},\\
P^z_{j,j+1} &= \frac{1}{3}\frac{I^z_4 A_1}{\Delta\left|B_{j,j+1}\right|}\left(\vec{e}_{j,j+1}\times(\vec{e}_j\times\vec{e}_{j+1})\right)\big|_z + \frac{1}{3}\frac{I^z_4 A_2}{\Delta\left|B_{j,j+1}\right|}\\
&\quad\times(\sin\theta_j\cos\theta_{j+1}\sin\phi_j + \cos\theta_j\sin\theta_{j+1}\sin\phi_{j+1}), \quad (21)
\end{aligned}$$

where $B_{j,j+1} = A_1\alpha_{j,j+1} + A_2\beta_{j,j+1}$, and $\alpha_{j,j+1}$ and $\beta_{j,j+1}$ are given as follows,

$$\begin{aligned}
\alpha_{j,j+1} &= \sin\frac{\theta_j}{2}\sin\frac{\theta_{j+1}}{2} + \cos\frac{\theta_j}{2}\cos\frac{\theta_{j+1}}{2}\mathrm{e}^{-\mathrm{i}(\phi_j-\phi_{j+1})},\\
\beta_{j,j+1} &= \mathrm{i}\left(\sin\frac{\theta_j}{2}\sin\frac{\theta_{j+1}}{2} - \cos\frac{\theta_j}{2}\cos\frac{\theta_{j+1}}{2}\mathrm{e}^{-\mathrm{i}(\phi_j-\phi_{j+1})}\right), \quad (22)
\end{aligned}$$

by replacing ϕ_1 and ϕ_2 in equation (14) by ϕ_j and ϕ_{j+1} respectively. And other parameters are defined as

$$\begin{aligned}
I^y_1 &= V_3 I^y_{yz,z} + V_4 I^y_{zx,z},\\
I^y_2 &= -V_1 I^y_{xy,x} + V_2 I^y_{xy,y} + V_3 I^y_{zx,z} - V_4 I^y_{yz,z},\\
I^y_3 &= V_1 I^y_{xy,x} + V_2 I^y_{xy,y} + V_3 I^y_{zx,z} + V_4 I^y_{yz,z},\\
I^z_4 &= V_2 I^z_{yz,y} + V_4 I^z_{xy,z} - V_1 I^z_{yz,x}. \quad (23)
\end{aligned}$$

Each component in the electric polarization $\vec{P}_{j,j+1}$ contains two parts, one part can be written in terms of $\vec{e}_j \times \vec{e}_{j+1}$ which has been predicted in [9], the other part is related to the bond distortion and depends on the bending angle φ. We denote the second part subject to bond distortion as 'lattice-mediated', to distinguish it from the 'spin-current' polarization in the first part. Note that, both lattice-mediated contribution and spin-current contribution are of the order of V/Δ and comparable to each other when φ is large enough.

We would like to point out that the vanishing x-component of the electric polarization $P^x_{j,j+1}$ origin from the mirror symmetry, namely, the two M atoms locate mirror-symmetrically about the yz plane across the oxygen atom and the Γ_7 manifold in equation (2) which stays unchanged under the mirror operation $x \to -x$. This symmetry, which is also present in Katsura *et al*'s model [9] but not in Jia *et al*'s model [10], will make the x-component polarization vanish.

For *double-hole situation* when $E_F > E_2$, two lowest states $|1\rangle$ and $|2\rangle$ are involved. Using equations (19), (B.1) and (B.2), we can easily calculate the electric polarization $\vec{P}_{j,j+1}$, which results in

$$\begin{aligned}
P^x_{j,j+1} &= 0,\\
P^y_{j,j+1} &= -\frac{2}{3}\frac{I^y_1 A_1 + I^y_2 A_2}{\Delta^2}\left(\vec{e}_{j,j+1}\times(\vec{e}_j\times\vec{e}_{j+1})\right)\big|_y\\
&\quad - \frac{4}{3}\frac{I^y_3}{\Delta}\left(1+\frac{C}{\Delta}\right) + \frac{4}{3}\frac{I^y_2 A_1\left|\alpha_{j,j+1}\right|^2 + I^y_1 A_2\left|\beta_{j,j+1}\right|^2}{\Delta^2},\\
P^z_{j,j+1} &= -\frac{2}{3}\frac{I^z_4 A_1}{\Delta^2}\left(\vec{e}_{j,j+1}\times(\vec{e}_j\times\vec{e}_{j+1})\right)\big|_z - \frac{2}{3}\frac{I^z_4 A_2}{\Delta^2}\\
&\quad\times(\sin\theta_j\cos\theta_{j+1}\sin\phi_j + \cos\theta_j\sin\theta_{j+1}\sin\phi_{j+1}). \quad (24)
\end{aligned}$$

To derive $\vec{P}_{j,j+1}$, we have made the approximation $\langle 1|1\rangle^{-1} \approx 1 + (C - |B|)/\Delta$ and $\langle 2|2\rangle^{-1} \approx 1 + (C + |B|)/\Delta$. Similar to the single-hole situation, the electric polarization can be divided into two parts, the lattice-mediated contribution and the spin-current contribution. However, it is different from the single-hole situation in that the spin-current contribution is of the order of $(V/\Delta)^3$ while the lattice-mediated part is of the order of V/Δ. This is because the electric polarization contains two parts from states $|1\rangle$ and $|2\rangle$, respectively, which tend to each other [9]. So the lattice-mediated

contribution will dominate over spin-current contribution when φ is large enough. It is worth noting that when $\varphi = 0$, the lattice-mediated contribution vanishes and the standard spin-current form in [9] can be reproduced from equations (13) and (23).

3.2. Four-atom M–O_2–M cluster

For a four-atom M–O_2–M cluster, only the spin-current polarization contributes to the electric polarization while lattice-mediated polarization vanishes. Using the results in appendix C, one can straightforwardly calculate the electric polarization.

For the *single-hole situation*, one obtains that

$$\begin{aligned} P^x_{j,j+1} &= 0, \\ P^y_{j,j+1} &= \frac{2}{3}\frac{I^y_1}{\Delta}\frac{A_1}{|A_1|}\frac{\left(\vec{e}_{j,j+1}\times(\vec{e}_j\times\vec{e}_{j+1})\right)\big|_y}{|\alpha_{j,j+1}|}, \\ P^z_{j,j+1} &= \frac{2}{3}\frac{I^z_4}{\Delta}\frac{A_1}{|A_1|}\frac{\left(\vec{e}_{j,j+1}\times(\vec{e}_j\times\vec{e}_{j+1})\right)\big|_z}{|\alpha_{j,j+1}|}, \end{aligned} \tag{25}$$

where $\alpha_{j,j+1}$ is given in equation (22).

For the *double-hole situation*, one obtains that

$$\begin{aligned} P^x_{j,j+1} &= 0, \\ P^y_{j,j+1} &= -\frac{8}{3}\frac{I^y_1 A_1}{\Delta^2}\left(\vec{e}_{j,j+1}\times(\vec{e}_j\times\vec{e}_{j+1})\right)\big|_y, \\ P^z_{j,j+1} &= -\frac{8}{3}\frac{I^z_4 A_1}{\Delta^2}\left(\vec{e}_{j,j+1}\times(\vec{e}_j\times\vec{e}_{j+1})\right)\big|_z. \end{aligned} \tag{26}$$

One sees that lattice-mediated contribution to the electric polarization is cancelled due to the reflection symmetry between two oxygen atoms in such a M–$O_{1(2)}$–M cluster. The amplitude of the spin-current polarizations is anisotropic which is different from widely used isotropic form [9]. Recently, building on the tight-binding model given by Jia *et al* [10, 11], Xiang *et al* investigated a four-atom M–O_2–M cluster and observed this anisotropy numerically [31].

4. Chain models and electric orders

We go further to investigate different chains formed by three-atom M–O–M clusters or four-atom M–O_2–M clusters and study possible electric orders in such chains. Since most multiferroics are insulators, relevant electrons are localized within clusters, we may neglect electron hopping between clusters and use relevant local states $|1\rangle$ and $|2\rangle$ obtained from cluster models in the previous section to calculate the electric polarization $\vec{P}$ within each cluster.

4.1. Uniform bending M–O–M chain

Firstly, we consider the uniform bond distortion chain model shown in figure 5. In this case, all the bridge oxygen atoms deviate from the spin chain formed by transition metal atoms in the same direction and with the same bond-bending angle φ. This type of bond distortion may be ascribed to

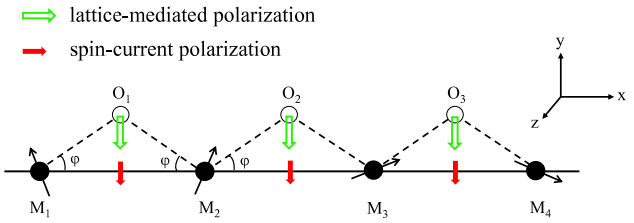

Figure 5. A sketch of the uniform bending M–O–M chain. All the bridge oxygen atoms deviate from the transition metal atoms chain in the same direction and lie within the *xy*-plane. And the spin spiral plane is the *xy*-plane. The spin-current and lattice-mediated polarization are denoted by red and green arrows, respectively.

the DM interaction related to spiral spin ordering, where the spin-helicity vector has the same sign for all pairs of neighboring spins. In the case of transverse-spiral ordering, the DM coupling pushes negative oxygen ions in the same direction [5].

It is easy to see that ferroelectric order will form in this kind of chains. To illustrate it, we assume all the magnetic moments from transition metal ions lie in the *xy*-plane and are spiral ordered in the same plane as shown in figure 5. In this case, from equations (21) and (24), we have $P^x_{j,j+1} = P^z_{j,j+1} = 0$, and then $P^y_{j,j+1}$ does not depend on-site index j.

For the single hole,

$$\begin{aligned} P^y_{j,j+1} = {} & \frac{1}{3}\frac{I^y_1 A_1 + I^y_2 A_2}{\Delta}\frac{\sin(\Delta\phi)}{\left|A_1\cos\frac{\Delta\phi}{2} - A_2\sin\frac{\Delta\phi}{2}\right|} \\ & - \frac{2}{3}\frac{I^y_3}{\Delta} - \frac{2}{3}\frac{I^y_2 A_1\left|\cos\frac{\Delta\phi}{2}\right|^2 + I^y_1 A_2\left|\sin\frac{\Delta\phi}{2}\right|^2}{\Delta\left|A_1\cos\frac{\Delta\phi}{2} - A_2\sin\frac{\Delta\phi}{2}\right|}, \end{aligned} \tag{27}$$

while for the double hole,

$$\begin{aligned} P^y_{j,j+1} = {} & -\frac{2}{3}\frac{I^y_1 A_1 + I^y_2 A_2}{\Delta^2}\sin(\Delta\phi) - \frac{4}{3}\frac{I^y_3}{\Delta}\left(1 + \frac{C}{\Delta}\right) \\ & + \frac{4}{3}\frac{I^y_2 A_1\left|\cos\frac{\Delta\phi}{2}\right|^2 + I^y_1 A_2\left|\sin\frac{\Delta\phi}{2}\right|^2}{\Delta^2}, \end{aligned} \tag{28}$$

with $\Delta\phi = \phi_j - \phi_{j+1}$.

4.2. Staggered bending M–O–M chain

There also exist some materials with staggered bending M–O–M chains as shown in figure 6. For instance, the Mn–O–Mn–O–Mn bonding along the $\langle 110\rangle$ direction forms a zigzag chain due to alternative rotation and tilt of the MnO_6 octahedra in some perovskite rare earth manganese oxides $RMnO_3$ [36].

In this case, spin-current polarization and lattice-mediated polarization may form different orders. To illustrate it, we still assume all the magnetic moments from transition metal ions lie in the *xy*-plane and are spiral ordered as shown in figure 6. In this case, $P^x_{j,j+1} = P^z_{j,j+1} = 0$. $P^y_{j,j+1}$ contains two parts, spin-current polarization $P^{sc,y}_{j,j+1}$ and

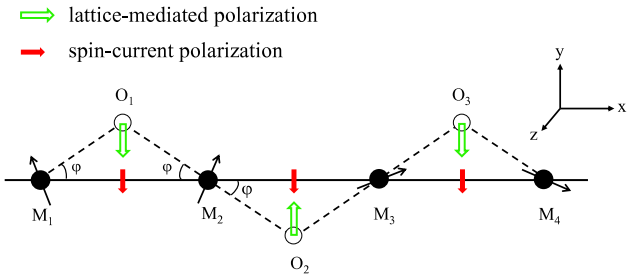

Figure 6. A sketch of the staggered M–O–M chain. The neighbor oxygen atoms of a given magnetic metal atom displace towards opposite directions. The spin-current polarization is uniform in each M–O–M cluster (red arrows), while lattice-mediated polarization is staggered (green arrows).

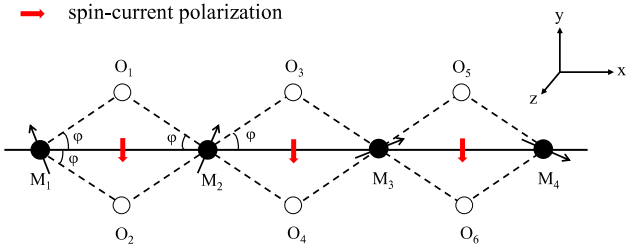

Figure 7. A schematic edge-shared MO_2 chain. The bridge oxygen atoms are symmetrically located beside the two sides of the magnetic metal atoms chain. In this case, the lattice-mediated contribution of the electric polarization is exactly cancelled. The nonvanish part of the polarization arise from the spin current, indicated by red arrows.

lattice-mediated polarization $P^{\mathrm{lm},y}_{j,j+1}$,

$$P^{y}_{j,j+1} = P^{\mathrm{sc},y}_{j,j+1} + P^{\mathrm{lm},y}_{j,j+1}. \tag{29}$$

For the single hole,

$$P^{\mathrm{sc},y}_{j,j+1} = \frac{1}{3}\frac{I^y_1 A_1 + I^y_2 A_2}{\Delta}\frac{\sin(\Delta\phi)}{\left|A_1\cos\frac{\Delta\phi}{2} + (-1)^j A_2 \sin\frac{\Delta\phi}{2}\right|},$$

$$P^{\mathrm{lm},y}_{j,j+1} = (-1)^j\frac{2}{3}\frac{I^y_3}{\Delta} + (-1)^j\frac{2}{3}\frac{I^y_2 A_1\left|\cos\frac{\Delta\phi}{2}\right|^2 + I^y_1 A_2\left|\sin\frac{\Delta\phi}{2}\right|^2}{\Delta\left|A_1\cos\frac{\Delta\phi}{2} + (-1)^j A_2\sin\frac{\Delta\phi}{2}\right|} \tag{30}$$

while for the double hole,

$$P^{\mathrm{sc},y}_{j,j+1} = -\frac{2}{3}\frac{I^y_1 A_1 + I^y_2 A_2}{\Delta^2}\sin(\Delta\phi),$$

$$P^{\mathrm{lm},y}_{j,j+1} = (-1)^j\frac{4}{3}\frac{I^y_3}{\Delta}\left(1+\frac{C}{\Delta}\right) + (-1)^{j+1}\frac{4}{3}\frac{I^y_2 A_1\left|\cos\frac{\Delta\phi}{2}\right|^2 + I^y_1 A_2\left|\sin\frac{\Delta\phi}{2}\right|^2}{\Delta^2}, \tag{31}$$

so that spin-current polarization is uniform and forms ferroelectric order while lattice-mediated polarization is staggered and forms antiferroelectric order. The total electric polarization is *'ferrielectric ordered'*.

4.3. Symmetric M–O_2–M chain

Finally, we consider a symmetric M–O_2–M chain shown in figure 7, which is made of four-atom M–O_2–M clusters. Such symmetric M–O_2–M chains exist in two prominent examples of multiferroic compound, namely, $LiCu_2O_2$ [25, 26] and $LiCuVO_4$ [27], which crystallize as one-dimensional chains of the edge-sharing CuO_4 plaquettes.

In this kind of chains, lattice-mediated polarization vanishes and spin-current polarization may form ferroelectric order. Assuming all the magnetic moments from transition metal ions lie in the *xy*-plane and are spiral ordered as shown in figure 7, we obtain $P^{x}_{j,j+1} = P^{z}_{j,j+1} = 0$ and

$$P^{y}_{j,j+1} = \frac{2}{3}\frac{I^y_1 A_1}{\Delta\,|A_1|}\frac{\sin(\Delta\phi)}{\left|\cos\frac{\Delta\phi}{2}\right|}, \tag{32}$$

in the single-hole situation and

$$P^{y}_{j,j+1} = -\frac{8}{3}\frac{I^y_1 A_1}{\Delta^2}\sin(\Delta\phi), \tag{33}$$

in the double-hole situation.

5. Discussions

In this section, we shall discuss the relation between magnetism-driven electric polarization and lattice-driven electric polarization, and then apply our theory to multiferroic copper oxides.

Lattice-driven electric polarization[1]: As shown in figure 5, the negatively charged oxygens coherently displace away from the magnetic chain formed by M ions. This shift will generate a net *lattice-driven* electric polarization P^{ld} directing from the oxygen ions to the M ions chain. The polarization P^{ld} can be evaluated as long as the p–d hybridizations $t_{\mathrm{pd}\sigma}$ and $t_{\mathrm{pd}\pi}$ and the geometry of the lattice are specified (details are given in appendix E). We shall compare this lattice-driven electric polarization (P^{ld}) with the two parts of magnetism-driven electric polarization studied in this paper, say, lattice-mediated polarization (P^{lm}) and spin-current polarization (P^{sc}). To do this, we restrict ourselves to the double-hole situation and choose the following parameters, $t_{\mathrm{pd}\sigma}/t_{\mathrm{pd}\pi} = -2$, [40] $\Delta = 2$ eV, $\sin(\Delta\phi) = \sin(0.28\pi)$ [11, 13, 15], typical M–O separation $R_{\mathrm{M-O}} = 4a_0$ (a_0 is the Bohr radius). The Clementi–Raimondi effective charges are chosen as $Z^{\mathrm{eff}}_{\mathrm{O}} = 4.45$ and $Z^{\mathrm{eff}}_{\mathrm{M}} = 10.53$ for O^{2-} and M ions, respectively. To calculate the electric polarization, we adopt a cubic lattice with lattice constant $a = 5$ Å and assume that each unit cell contains only one M_1–O–M_2 cluster. The results are shown in figure 8 where electric polarizations are plotted as

[1] The definition of the lattice-driven polarization in this work is a purely electronic origin, which is different with the definition of that in [16].

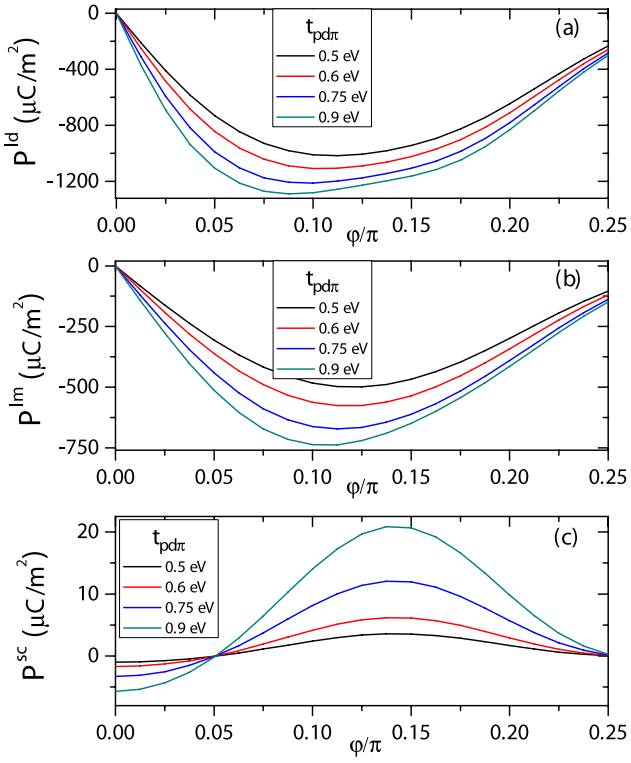

Figure 8. The φ-dependence of electric polarizations in uniform bending M–O–M chains (see figure 5). (a) Lattice-driven electric polarization. (b) Lattice-mediated polarization. (c) Spin-current polarization.

functions of bond-bending angle φ. For a typical φ, $P^{ld} \sim 10^2\ \mu C\ m^{-2}$, while $P^{lm} \sim 10^2\ \mu C\ m^{-2}$ and $P^{sc} \sim 10\ \mu C\ m^{-2}$. The lattice-mediated polarization keeps in parallel with the lattice-driven polarization for any bond-bending angle φ while the spin-current polarization may vary with φ and be in parallel or anti-parallel to the lattice-driven polarization. Moreover, the spin-current polarization depends on spin configuration and can be neither parallel nor anti-parallel to lattice-driven polarization. Upon these observations, we conclude that lattice-driven polarization is cooperative with lattice-mediated polarization while spin-current polarization may be either competitive or cooperative, depending on the spin configuration and the bond-bending angle.

Note that lattice-driven polarization P^{ld} in figure 8(a) is overestimated since we chose the maximum electric polarization in all the possible valences for magnetic transition metal and oxygen ions. It is also worth noting that although P^{ld} and P^{lm} dominate over P^{sc} at finite φ in uniform bending chains as shown in figure 8, P^{sc} will be dominating at small φ or in symmetric M–O_2–M chains.

Multiferroic copper oxides: Then we shall apply our theory to several copper oxides, including $LiCuVO_4$, $LiCu_2O_2$ and $NaCu_2O_2$, where magnetic copper ions Cu^{2+} and oxygen ions O^{2-} form symmetric M–O_2–M chain as shown in figure 7.

There are two prominent compounds which can be described as symmetric M–O_2–M chains, $LiCu_2O_2$ and $LiCuVO_4$. Both of them are characterized by edge-sharing CuO_4 plaquettes, forming spiral spin orders and emerging electric polarization at low temperature. The electric polarization in these two compounds is relatively weak comparing with manganites, $\sim$10 μC m^{-2}, and shows strong anisotropy. There is another interesting material $NaCu_2O_2$, which is isostructural to $LiCu_2O_2$ while Li is substituted by Na. Although $NaCu_2O_2$ also exhibits helical magnetic order at low temperature [41–43], no electric polarization has been observed in it within the experimental sensitivity ($<$0.3 μC m^{-2}) [44, 45].

It is noted that, although Katsura *et al*'s spin-current model (equation (1)) was developed in t_{2g} systems originally [9], its applicability to e_g systems has been confirmed experimentally [26, 30] and theoretically [11, 13, 46]. However, Katsura *et al*'s theory cannot account for the striking anisotropy of the polarization observed in $LiCu_2O_2$ [25, 26] and $LiCuVO_4$ [28, 29], and the absence of polarization in $NaCu_2O_2$ [44, 45]. We shall apply our theory to these prototypical compounds to make qualitative comparison with the experimental observations and address the issue of 'missing multiferroicity' in $NaCu_2O_2$ in the rest of this section.

As mentioned in section 3.2, the lattice-mediated contribution is exactly cancelled in a symmetric M–O_2–M cluster, and the electric polarization comes from the spin current only. In contrast to the widely used isotropic form of equation (1), the spin-current form of electric polarization in the symmetric M–O_2–M cluster is anisotropic in general, which is in accord with the experimental findings [28, 29, 25, 26] and density functional calculations [46]. The magnitude of the electric polarization depends on the bond-bending angle φ and vanishes at $\varphi = \pi/4$. Note that the spin-current form will recover isotropic in the absence of bond distortion, say, $\varphi = 0$.

In figure 9, we plot y- and z-components of electric polarization as functions of bond-bending angle φ in the presence of xy- and zx-plane spin spiral order, respectively. One sees that the polarization is sensitive to the bond-bending angle φ and is anisotropic. In realistic materials, the bond angles of Cu–O–Cu in $LiCuVO_4$, $LiCu_2O_2$, and $NaCu_2O_2$ are 95° [28], 94° [26], and 92.9° [41, 42], respectively, corresponding to bond-bending angles $\varphi = 42.5°, 43°$, and 43.6°, which are all close to $\varphi = \pi/4$. As shown in the figure 9, the electric polarization decreases and ultimately vanishes when φ approaches $\pi/4$. Indeed, experiments clearly indicated that the electric polarization in $LiCuVO_4$ is stronger than that of $LiCu_2O_2$. Moreover, the bond-bending angle φ in $NaCu_2O_2$ is closer to $\pi/4$ than that of $LiCuVO_4$ and $LiCu_2O_2$, resulting in weaker electric polarization which is difficult to be observed.

For comparison, we also list calculated electric polarizations for these three compounds in table 1 using their concrete parameters, such as the lattice constants, pitch angles and bond-bending angles φ. For example, the pitch angles for $LiCuVO_4$, $LiCu_2O_2$ and $NaCu_2O_2$ are 84.2° [28, 29], 62.6° [26], and 81.7° [45], respectively. Corresponding $R_{Cu–O}$ ($R_{Cu–O}$ is the distance of the Cu–O bond along the Cu–Cu chain) are 1.446 Å [49], 1.43 Å [26], and 1.465 Å [45], respectively. Other relevant parameters are the same as

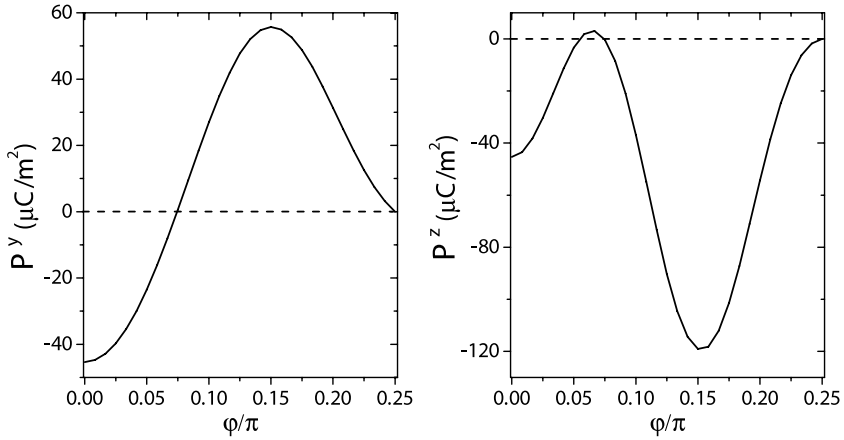

Figure 9. The φ-dependence of y- and z-components of electric polarization in the presence of xy- and zx-plane spin spiral order, respectively in symmetric M–O_2–M chains (see figure 7). A typical set of parameters are chosen for Cu^{2+} oxides [47], $t_{pd\pi} = 0.75$ eV, $t_{pd\sigma} = -1.85$ eV, $\Delta = 3$ eV. The Clementi–Raimondi effective charges $Z_O^{eff} = 4.45$ and $Z_{Cu}^{eff} = 13.2$ are used for O^{2-} and Cu^{2+} ions, respectively [48]. We use $R_{Cu-O} = 1.446$ Å for $LiCuVO_4$ [49]. To calculate electric polarization, we use the facts that the volume of the unit cell is 284.1 $Å^3$ and each unit cell contains four Cu–O_2–Cu clusters.

Table 1. The a- and c-components of electric polarizations in $LiCuVO_4$, $LiCu_2O_2$ and $NaCu_2O_2$ in the presence of ab- and bc-plane spin spiral orders. The values in parentheses correspond to experimental data.

		Polarization (μC m^{-2})	
Materials	φ (deg)	P_a (ab)	P_c (bc)
$LiCuVO_4$ [28, 29]	42.5	5.8 (43)	4.3 (10)
$LiCu_2O_2$ [25, 26]	43	4.4 (8)	3.8 (4)
$NaCu_2O_2$ [45]	43.6	2.1 (?[a])	0.8 (0)

[a] Currently no experimental data is available.

those in figure 9. The values in parentheses in table 1 are experimental data. The decreasing electric polarization with φ approaching $\pi/4$ is qualitatively in agreement with experimental observation. For the $NaCu_2O_2$ compound in the presence of bc-plane spin spiral order [41, 43], we find that P_c is extremely weak and hard to detect [45]. To our knowledge, there is no experimental report on electric polarization in the presence of ab-plane spin spiral order, which may be tunable under external field. Our theory predicts a finite electric polarization (~ 2 μC m^{-2}) oriented along the a-axis in the presence of ab-plane spin spiral order. This prediction can be tested in future experiments for $NaCu_2O_2$. Thus, the effect of bond distortion on the magnetic-driven polarization may provide a clue to clarify the anisotropy of the electric polarization observed in $LiCuVO_4$ and $LiCu_2O_2$ and to elucidate the puzzle of non-multiferroicity in $NaCu_2O_2$.

6. Conclusion

In this paper, we have studied how the distortion of M–O–M bonds affect the lowest lying electronic states thereby the electric polarization in multiferroic magnets. We calculated relevant low lying electronic states and electric polarization for three-atom M–O–M clusters and four-atom M–O_2–M clusters, respectively. Our calculations, indeed, showed that the M–O–M bond distortion has significant impacts on the induced electric polarization in multiferroics. It turns out that the electric polarization contains two parts in general: the spin-current polarization which can be written in terms of $\vec{e}_{i,j} \times (\vec{e}_i \times \vec{e}_j)$ and the lattice-mediated polarization which exists only when the M–O–M bond angle deviates away from 180°. Both the magnitude of the spin-current and the lattice-mediated polarization are influenced by the bond distortion. Furthermore, spin-current polarization exhibits anisotropic behavior which is in contrast to the widely used isotropic form proposed by Katsura *et al* [9], while the lattice-mediated polarization is sensitive to the bond distortion configuration. We have then further explored three kinds of chain models made of different clusters where magnetic moments are spiral ordered. In such chains, ferroelectric or ferrielectric orderings may emerge depending on the geometry of the chain.

We have also discussed, in detail, the relation between magnetic-driven electric polarization and lattice-driven electric polarization in the presence of bond distortion. We found that the lattice-driven polarization is cooperative with lattice-mediated polarization while spin-current polarization may be either competitive or cooperative, depending on the spin configuration and the bond-bending angle. We have applied our theory to several multiferroic copper oxides which can be viewed as symmetric M–O_2–M chains. It is shown that the anisotropic spin-current polarization is highly sensitive to the bond-bending angle φ. Especially, the φ is much closer to $\pi/4$, the weaker the electric polarization, which are in very good qualitative agreement with the behavior of electric polarization observed in multiferroics copper oxides. Therefore, it suggests that the bond distortion effect may play a crucial role to explain the peculiarities of the electric polarization observed in $LiCu_2O_2$ and $LiCuVO_4$, i.e., anisotropy and φ-dependent trends of polarization, and to elucidate the puzzle of 'missing multiferroicity' in $NaCu_2O_2$.

Summarizing, we show that the M–O–M bond distortion may affect electric polarization in multiferroics significantly and the possibilities for ferroelectric and ferrielectric ordering

are discussed. We also apply the theory to multiferroics copper oxides, which is in agreement with experiments, qualitatively.

Acknowledgments

This work is supported by the National Basic Research Program of China (973 Program, No. 2011CBA00103), NSFC (Grant No. 11074216, 10874149 and 11074218), RFDP (No. 20100101120002), PCSIRT (No. IRT0754), the Doctoral Fund of the Ministry of Education of China, and the Fundamental Research Funds for the Central Universities in China.

Appendix A. Coefficients $A_{(j)}^{i\sigma}$ and $B_{(j)}^{i\sigma}$ in equations (5*a*) and (5*b*)

In this appendix we shall derive coefficients $A_{(j)}^{i\sigma}$ and $B_{(j)}^{i\sigma}$ in equations (5*a*) and (5*b*). For the parallel state $|P_j\rangle$ and corresponding coefficients $A_{(j)}^{i\sigma}$, we combine equations (4*a*) and (5*a*) to have

$$\sin\frac{\theta_j}{2}|a\rangle + e^{i\phi_j}\cos\frac{\theta_j}{2}|b\rangle = \sum_{i\sigma} A_{(j)}^{i\sigma}\left|d_{i\sigma}^{(j)}\right\rangle. \tag{A.1}$$

Using the relation equation (2), we obtain $A_{(j)}^{i\sigma}$ as follows,

$$A_{(j)}^{xy,\uparrow} = \frac{1}{\sqrt{3}}\sin\frac{\theta_j}{2}, \tag{A.2a}$$

$$A_{(j)}^{xy,\downarrow} = \frac{1}{\sqrt{3}}e^{i\phi_j}\cos\frac{\theta_j}{2}, \tag{A.2b}$$

$$A_{(j)}^{yz,\uparrow} = -\frac{1}{\sqrt{3}}e^{i\phi_j}\cos\frac{\theta_j}{2}, \tag{A.2c}$$

$$A_{(j)}^{yz,\downarrow} = \frac{1}{\sqrt{3}}\sin\frac{\theta_j}{2}, \tag{A.2d}$$

$$A_{(j)}^{zx,\uparrow} = \frac{1}{\sqrt{3}}ie^{i\phi_j}\cos\frac{\theta_j}{2}, \tag{A.2e}$$

$$A_{(j)}^{zx,\downarrow} = \frac{1}{\sqrt{3}}i\sin\frac{\theta_j}{2}. \tag{A.2f}$$

Similarly, we obtain coefficients $B_{(j)}^{i\sigma}$ for the anti-parallel state $|AP_j\rangle$ as follows,

$$B_{(j)}^{xy,\uparrow} = \frac{1}{\sqrt{3}}\cos\frac{\theta_j}{2}, \tag{A.3a}$$

$$B_{(j)}^{xy,\downarrow} = -\frac{1}{\sqrt{3}}e^{i\phi_j}\sin\frac{\theta_j}{2}, \tag{A.3b}$$

$$B_{(j)}^{yz,\uparrow} = \frac{1}{\sqrt{3}}e^{i\phi_j}\sin\frac{\theta_j}{2}, \tag{A.3c}$$

$$B_{(j)}^{yz,\downarrow} = \frac{1}{\sqrt{3}}\cos\frac{\theta_j}{2}, \tag{A.3d}$$

$$B_{(j)}^{zx,\uparrow} = -\frac{1}{\sqrt{3}}ie^{i\phi_j}\sin\frac{\theta_j}{2}, \tag{A.3e}$$

$$B_{(j)}^{zx,\downarrow} = \frac{1}{\sqrt{3}}i\cos\frac{\theta_j}{2}. \tag{A.3f}$$

Appendix B. Lowest lying eigenstates for the three-atom M–O–M cluster

We calculate the eigenvectors for two lowest lying eigenstates $|1\rangle$ and $|2\rangle$ in a three-atom M–O–M cluster in this appendix. The Hilbert space contains states $|P_j\rangle$, $(j = 1, 2)$ and $p_{\mu,\sigma}$ $(\mu = x, y, z,\ \sigma = \uparrow, \downarrow)$. Assuming $V \ll \Delta$ and treating H_t as a perturbation to H_Δ, we obtain the two eigenvectors $|1\rangle$ and $|2\rangle$ up to the second order perturbation,

$$\begin{aligned}|1\rangle = &-\frac{B}{\sqrt{2}|B|}\\ &\times\left[|P_1\rangle - \frac{1}{\Delta}\sum_\sigma\left(A_{(1)}^{xy,\sigma}\left(V_1|p_{x,\sigma}\rangle + V_2|p_{y,\sigma}\rangle\right)\right.\right.\\ &\left.\left.+ (V_3A_{(1)}^{zx,\sigma} + V_4A_{(1)}^{yz,\sigma})|p_{z,\sigma}\rangle\right)\right]\\ &+\frac{1}{\sqrt{2}}\left[|P_2\rangle - \frac{1}{\Delta}\sum_\sigma\left(A_{(2)}^{xy,\sigma}\left(V_1|p_{x,\sigma}\rangle - V_2|p_{y,\sigma}\rangle\right)\right.\right.\\ &\left.\left.+ (-V_3A_{(2)}^{zx,\sigma} + V_4A_{(2)}^{yz,\sigma})|p_{z,\sigma}\rangle\right)\right],\end{aligned} \tag{B.1}$$

with $E_1 = 2(C - |B|)$, and

$$\begin{aligned}|2\rangle = &\frac{B}{\sqrt{2}|B|}\left[|P_1\rangle - \frac{1}{\Delta}\sum_\sigma\left(^2A_{(1)}^{xy,\sigma}\left(V_1|p_{x,\sigma}\rangle + V_2|p_{y,\sigma}\rangle\right)\right.\right.\\ &\left.\left.+ (V_3A_{(1)}^{zx,\sigma} + V_4A_{(1)}^{yz,\sigma})|p_{z,\sigma}\rangle\right)\right]\\ &+\frac{1}{\sqrt{2}}\left[|P_2\rangle - \frac{1}{\Delta}\sum_\sigma\left(^2A_{(2)}^{xy,\sigma}\left(V_1|p_{x,\sigma}\rangle - V_2|p_{y,\sigma}\rangle\right)\right.\right.\\ &\left.\left.+ (-V_3A_{(2)}^{zx,\sigma} + V_4A_{(2)}^{yz,\sigma})|p_{z,\sigma}\rangle\right)\right],\end{aligned} \tag{B.2}$$

with $E_2 = 2(C + |B|)$, where parameters C and B are given in equations (12)–(14) in the main text, coefficients $A_{(j)}^{i\sigma}$ are given in equation (1.2). It is easy to verify that the states $|1\rangle$ and $|2\rangle$ are orthogonal to each other and their normalization factors are $\langle 1|1\rangle = 1 - (C - |B|)/\Delta$ and $\langle 2|2\rangle = 1 - (C + |B|)/\Delta$, respectively.

Appendix C. Lowest lying eigenstates for the four-atom M–O_2–M cluster

In this appendix, we calculate the eigenvectors for two lowest lying eigenstates $|1\rangle$ and $|2\rangle$ in a four-atom M–O_2–M cluster. In this situation, the Hilbert space contains states $|P_j\rangle$ $(j = 1, 2)$ and $p_{\mu,\sigma}^{(i)}$ $(i = 1, 2,\ \mu = x, y, z,\ \sigma = \uparrow, \downarrow)$. Up to the second order of $\frac{V}{\Delta}$, we obtain the two eigenvectors $|1\rangle$ and $|2\rangle$ as follows,

$$\begin{aligned}|1\rangle = &-\frac{A_1\alpha}{\sqrt{2}|A_1\alpha|}\\ &\times\left[|P_1\rangle - \frac{1}{\Delta}\sum_\sigma\left(A_{(1)}^{xy,\sigma}\left(V_1\left|p_{x,\sigma}^{(1)}\right\rangle + V_2\left|p_{y,\sigma}^{(1)}\right\rangle\right)\right.\right.\end{aligned}$$

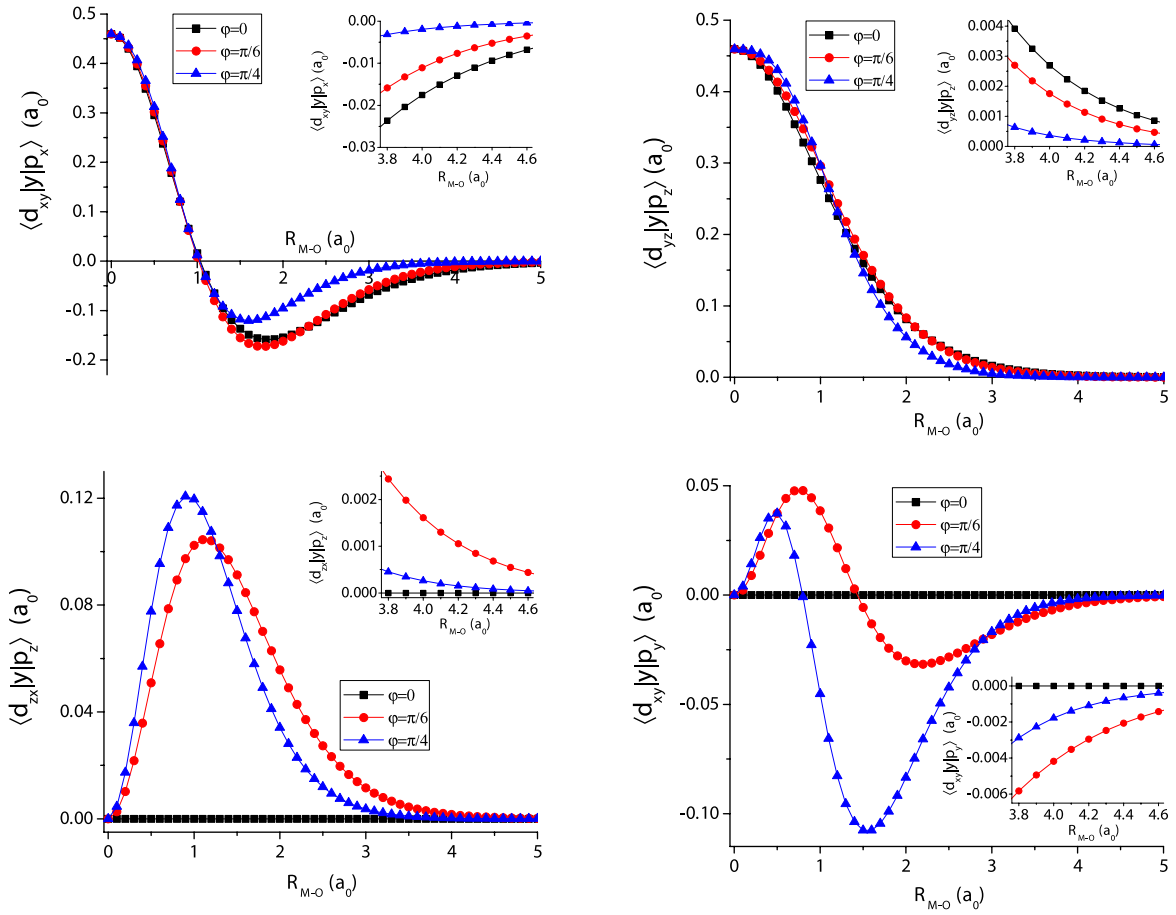

Figure D.1. Two-site dipole integrals $I^{y}_{\mu,\nu}$ against M–O separation $R_{\mathrm{M–O}}$ with various bond-bending angles. The inset in each figure shows the zoom in view of the integrals near typical M–O separation (i.e., $4a_0$, a_0 is the Bohr radius).

$$
\begin{aligned}
&+\left(V_3A^{zx,\sigma}_{(1)}+V_4A^{yz,\sigma}_{(1)}\right)\left|\mathrm{p}^{(1)}_{z,\sigma}\right\rangle\\
&-A^{xy,\sigma}_{(1)}\left(V_1\left|\mathrm{p}^{(2)}_{x,\sigma}\right\rangle-V_2\left|\mathrm{p}^{(2)}_{y,\sigma}\right\rangle\right)\\
&+\left(V_3A^{zx,\sigma}_{(1)}-V_4A^{yz,\sigma}_{(1)}\right)\left|\mathrm{p}^{(2)}_{z,\sigma}\right\rangle\Big)\Big]\\
&+\frac{1}{\sqrt{2}}\Bigg[|P_2\rangle-\frac{1}{\Delta}\sum_{\sigma}\Big(A^{xy,\sigma}_{(2)}\left(V_1\left|\mathrm{p}^{(1)}_{x,\sigma}\right\rangle-V_2\left|\mathrm{p}^{(1)}_{y,\sigma}\right\rangle\right)\\
&+\left(-V_3A^{zx,\sigma}_{(2)}+V_4A^{yz,\sigma}_{(2)}\right)\left|\mathrm{p}^{(1)}_{z,\sigma}\right\rangle\\
&-A^{xy,\sigma}_{(2)}\left(V_1\left|\mathrm{p}^{(2)}_{x,\sigma}\right\rangle+V_2\left|\mathrm{p}^{(2)}_{y,\sigma}\right\rangle\right)\\
&+\left(-V_3A^{zx,\sigma}_{(2)}-V_4A^{yz,\sigma}_{(2)}\right)\left|\mathrm{p}^{(2)}_{z,\sigma}\right\rangle\Big)\Bigg], \qquad \text{(C.1)}
\end{aligned}
$$

with $E_1 = 2(C - |A_1\alpha|)$, and

$$
\begin{aligned}
|2\rangle = &\frac{A_1\alpha}{\sqrt{2}\,|A_1\alpha|}\\
&\times\Bigg[|P_1\rangle-\frac{1}{\Delta}\sum_{\sigma}\Big(A^{xy,\sigma}_{(1)}\left(V_1\left|\mathrm{p}^{(1)}_{x,\sigma}\right\rangle+V_2\left|\mathrm{p}^{(1)}_{y,\sigma}\right\rangle\right)\\
&+\left(V_3A^{zx,\sigma}_{(1)}+V_4A^{yz,\sigma}_{(1)}\right)\left|\mathrm{p}^{(1)}_{z,\sigma}\right\rangle\\
&-A^{xy,\sigma}_{(1)}\left(V_1\left|\mathrm{p}^{(2)}_{x,\sigma}\right\rangle-V_2\left|\mathrm{p}^{(2)}_{y,\sigma}\right\rangle\right)\\
&+\left(V_3A^{zx,\sigma}_{(1)}-V_4A^{yz,\sigma}_{(1)}\right)\left|\mathrm{p}^{(2)}_{z,\sigma}\right\rangle\Big)\Bigg]\\
&+\frac{1}{\sqrt{2}}\Bigg[|P_2\rangle-\frac{1}{\Delta}\sum_{\sigma}\Big(A^{xy,\sigma}_{(2)}\left(V_1\left|\mathrm{p}^{(1)}_{x,\sigma}\right\rangle-V_2\left|\mathrm{p}^{(1)}_{y,\sigma}\right\rangle\right)\\
&+\left(-V_3A^{zx,\sigma}_{(2)}+V_4A^{yz,\sigma}_{(2)}\right)\left|\mathrm{p}^{(1)}_{z,\sigma}\right\rangle\\
&-A^{xy,\sigma}_{(2)}\left(V_1\left|\mathrm{p}^{(2)}_{x,\sigma}\right\rangle+V_2\left|\mathrm{p}^{(2)}_{y,\sigma}\right\rangle\right)\\
&+\left(-V_3A^{zx,\sigma}_{(2)}-V_4A^{yz,\sigma}_{(2)}\right)\left|\mathrm{p}^{(2)}_{z,\sigma}\right\rangle\Big)\Bigg], \qquad \text{(C.2)}
\end{aligned}
$$

with $E_2 = 2(C + |A_1\alpha|)$, where parameters C, A_1 and α are given in equations (12)–(14) in the main text, coefficients $A^{i\sigma}_{(j)}$ are given in equation(A.2). The normalization factors are $\langle 1|1\rangle = 1 - 2\,(C - |A_1\alpha|)\,/\Delta$ and $\langle 2|2\rangle = 1 - 2\,(C + |A_1\alpha|)\,/\Delta$.

Appendix D. Overlap dipole matrix elements $I^{\alpha}_{\mu,\nu}(\vec{a})$

From the definition of the overlap dipole matrix elements $I^{\alpha}_{\mu,\nu}(\vec{a})$ in equation (20), and using the mirror symmetry about the xy-plane ($z \to -z$), we find that the following matrix

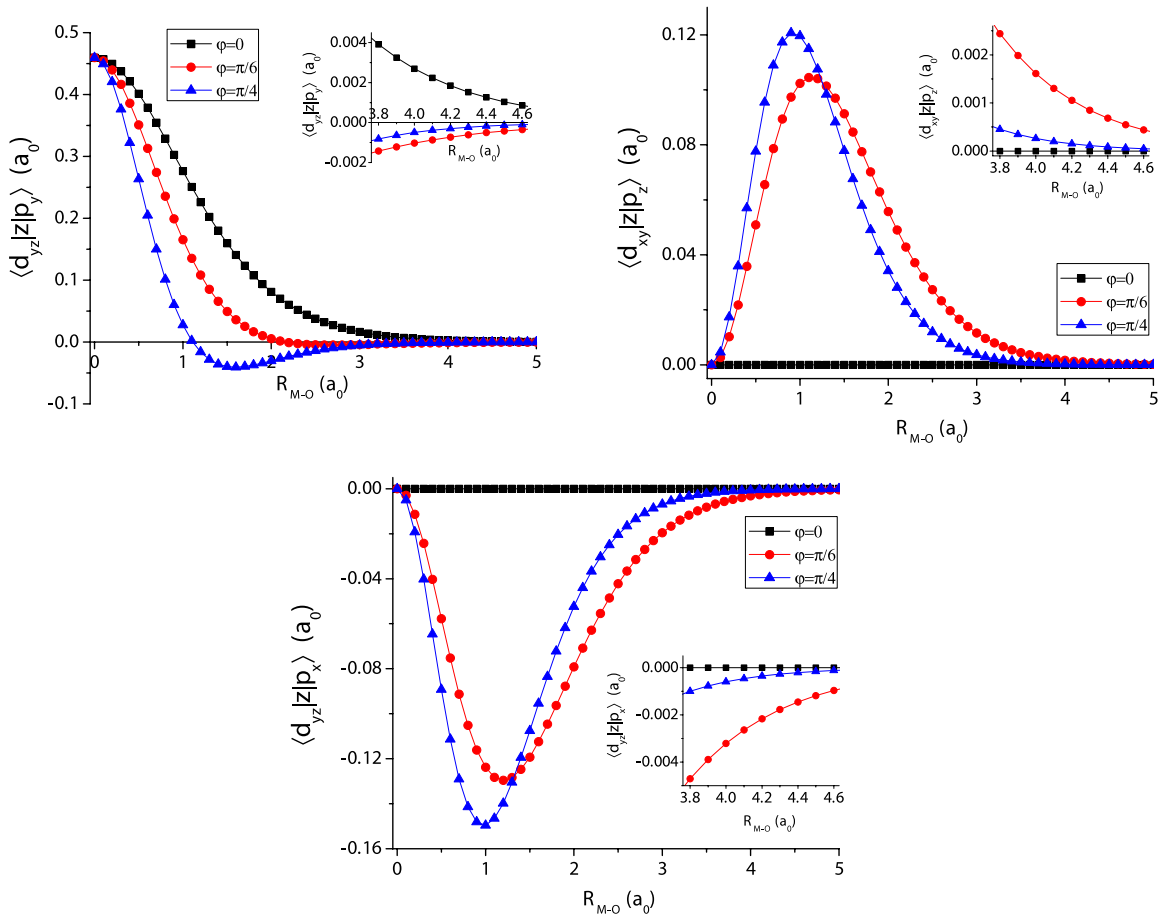

Figure D.2. Two-site dipole integrals $I^z_{\mu,\nu}$ against M–O separation $R_{\mathrm{M–O}}$ with various bond-bending angles. The inset in each figure shows the zoom in view of the integrals near typical M–O separation (i.e., $4a_0$).

elements vanish,

$$I^x_{xy,z} = I^x_{yz,x} = I^x_{yz,y} = I^x_{zx,x} = I^x_{zx,y} = 0,$$
$$I^y_{xy,z} = I^y_{yz,x} = I^y_{yz,y} = I^y_{zx,x} = I^y_{zx,y} = 0,$$
$$I^z_{xy,x} = I^z_{xy,y} = I^z_{yz,z} = I^z_{zx,z} = 0.$$

Then we study symmetry relations for nonvanishing $I^\alpha_{\mu,\nu}(\vec{a})$ with two vectors $\vec{a}$ and $\vec{b}$, where $\vec{a}$ and $\vec{b}$ lie within the xy-plane and are linked by symmetry $P_x(x \to -x)$ or $P_y(y \to -y)$. When $\vec{b} = P_x\vec{a}$ or $\vec{b} = P_y\vec{a}$, we have

$$I^x_{xy,y}(\vec{a}) = I^x_{xy,y}(\vec{b}), \qquad I^x_{xy,x}(\vec{a}) = -I^x_{xy,x}(\vec{b}),$$
$$I^x_{yz,z}(\vec{a}) = -I^x_{yz,z}(\vec{b}), \qquad I^x_{zx,z}(\vec{a}) = I^x_{zx,z}(\vec{b}),$$
$$I^y_{xy,x}(\vec{a}) = I^y_{xy,x}(\vec{b}), \qquad I^y_{xy,y}(\vec{a}) = -I^y_{xy,y}(\vec{b}),$$
$$I^y_{yz,z}(\vec{a}) = I^y_{yz,z}(\vec{b}), \qquad I^y_{zx,z}(\vec{a}) = -I^y_{zx,z}(\vec{b}),$$
$$I^z_{xy,z}(\vec{a}) = -I^z_{xy,z}(\vec{b}), \qquad I^z_{yz,x}(\vec{a}) = -I^z_{yz,x}(\vec{b}),$$
$$I^z_{yz,y}(\vec{a}) = I^z_{yz,y}(\vec{b}), \qquad I^z_{zx,x}(\vec{a}) = I^z_{zx,x}(\vec{b}),$$
$$I^z_{zx,y}(\vec{a}) = -I^z_{zx,y}(\vec{b}),$$

for nonvanishing $I^\alpha_{\mu,\nu}(\vec{a})$.

It turns out that relevant $I^\alpha_{\mu,\nu}(\vec{a})$'s in the main text include $I^z_{yz,y}$, $I^z_{xy,z}$, $I^z_{yz,x}$, $I^y_{xy,x}$, $I^y_{yz,z}$, $I^y_{zx,z}$, $I^y_{xy,y}$. We demonstrate the numerical evaluation for these integrals in figures D.1 and D.2, respectively. $R_{\mathrm{M–O}}$ is the M–O bond distance along the M–M chain. In this calculation, we have taken the hydrogen like radial-wavefunctions and the Clementi–Raimondi effective charges $Z^{\mathrm{eff}}_{\mathrm{O}} = 4.45$ and $Z^{\mathrm{eff}}_{\mathrm{M}} = 10.53$ for O^{2-} and Mn^{3+} ions respectively [48]. It is shown that, for typical M–O separation (i.e., $R_{\mathrm{M–O}} \sim 4a_0$, here a_0 is Bohr radius), $I^y_{xy,x}$ is one order of magnitude larger than those of other integrals. The separation between the M and O ions $R_{\mathrm{M–O}}$ not only yields violent variance on the magnitude of the overlap dipole integrals but also may change their signs.

Appendix E. Calculation details of the lattice-driven polarization P^{ld}

In this appendix, we present the calculation details of the lattice-driven polarization P^{ld} shown in figure 8(a). In order to calculate the lattice-driven electric polarization in the uniform bending M–O–M chain (see figure 5), we should calculate the electric dipole moment of the M_1–O–M_2 cluster in figure 3. The Hamiltonian describing the three-atom M_1–O–M_2 cluster is given by

$$H = H_{\mathrm{M}} + H_{\mathrm{O}} + H_{\mathrm{V}}, \tag{E.1}$$

with

$$H_{\rm M} = \sum_{a=xy,yz,zx;i=1,2} \varepsilon_{\rm d} {\rm d}_a^{\dagger(i)} {\rm d}_a^{(i)}, \tag{E.2}$$

$$H_{\rm O} = \sum_{b=x,y,z} \varepsilon_{\rm p} {\rm p}_b^{\dagger} {\rm p}_b, \tag{E.3}$$

$$\begin{aligned} H_{\rm V} = {} & V_1 {\rm p}_x^{\dagger} {\rm d}_{xy}^{(1)} + V_2 {\rm p}_y^{\dagger} {\rm d}_{xy}^{(1)} + V_3 {\rm p}_z^{\dagger} {\rm d}_{zx}^{(1)} + V_4 {\rm p}_z^{\dagger} {\rm d}_{yz}^{(1)} \\ & + V_1 {\rm p}_x^{\dagger} {\rm d}_{xy}^{(2)} - V_2 {\rm p}_y^{\dagger} {\rm d}_{xy}^{(2)} - V_3 {\rm p}_z^{\dagger} {\rm d}_{zx}^{(2)} \\ & + V_4 {\rm p}_z^{\dagger} {\rm d}_{yz}^{(2)} + {\rm H.c.}, \end{aligned} \tag{E.4}$$

where $\varepsilon_{\rm d}$ and $\varepsilon_{\rm p}$ represent the on-site energies of the d-orbitals in transition metal atoms and p-orbitals in oxygen atom in the hole picture, respectively. In $H_{\rm M}$, we consider just triply degenerate t_{2g} orbitals for simplicity. $H_{\rm V}$ describes the M–O hybridization depending on the d- and p-orbitals involved and V_i ($i = 1, 2, 3, 4$) are the same hybridization integrals defined in equation (10). In our model, there is no spin interaction, so we neglect the spin index. There are 9 coupled states, denoted by ${\rm d}_a^{(i)}$ ($a = xy, yz, zx$; $i = 1, 2$) and ${\rm p}_b$ ($b = x, y, z$). With these 9 states as basis, we write the Hamiltonian as the following matrix form

$$H = \begin{pmatrix} \varepsilon_{\rm d} & 0 & 0 & 0 & 0 & 0 & V_1 & V_2 & 0 \\ 0 & \varepsilon_{\rm d} & 0 & 0 & 0 & 0 & 0 & 0 & V_4 \\ 0 & 0 & \varepsilon_{\rm d} & 0 & 0 & 0 & 0 & 0 & V_3 \\ 0 & 0 & 0 & \varepsilon_{\rm d} & 0 & 0 & V_1 & -V_2 & 0 \\ 0 & 0 & 0 & 0 & \varepsilon_{\rm d} & 0 & 0 & 0 & V_4 \\ 0 & 0 & 0 & 0 & 0 & \varepsilon_{\rm d} & 0 & 0 & -V_3 \\ V_1 & 0 & 0 & V_1 & 0 & 0 & \varepsilon_{\rm p} & 0 & 0 \\ V_2 & 0 & 0 & -V_2 & 0 & 0 & 0 & \varepsilon_{\rm p} & 0 \\ 0 & V_4 & V_3 & 0 & V_4 & -V_3 & 0 & 0 & \varepsilon_{\rm p} \end{pmatrix}. \tag{E.5}$$

It can be diagonalized and the eigenvalues are

$$\varepsilon_1 = \varepsilon_2 = \varepsilon_3 = \varepsilon_{\rm d}, \tag{E.6}$$

$$\varepsilon_4^{\pm} = \tfrac{1}{2}\left(\varepsilon_{\rm d} + \varepsilon_{\rm p} \pm \sqrt{\Delta_0^2 + 8V_1^2}\right), \tag{E.7}$$

$$\varepsilon_5^{\pm} = \tfrac{1}{2}\left(\varepsilon_{\rm d} + \varepsilon_{\rm p} \pm \sqrt{\Delta_0^2 + 8V_2^2}\right), \tag{E.8}$$

$$\varepsilon_6^{\pm} = \tfrac{1}{2}\left(\varepsilon_{\rm d} + \varepsilon_{\rm p} \pm \sqrt{\Delta_0^2 + 8(V_3^2 + V_4^2)}\right), \tag{E.9}$$

where $\Delta_0 = \varepsilon_{\rm p} - \varepsilon_{\rm d}$ ($\Delta_0 > 0$, since $\varepsilon_{\rm p}$ and $\varepsilon_{\rm d}$ are hole energies) and the corresponding eigenvectors are

$$\psi_1 = \left(\frac{V_3}{V_4}{\rm d}_{yz}^{(1)} + {\rm d}_{zx}^{(2)}\right) \Big/ \left(1 + (V_3/V_4)^2\right)^{1/2}, \tag{E.10}$$

$$\psi_2 = \left(-{\rm d}_{yz}^{(1)} + {\rm d}_{yz}^{(2)}\right)/\sqrt{2}, \tag{E.11}$$

$$\psi_3 = \left(-\frac{V_3}{V_4}{\rm d}_{yz}^{(1)} + {\rm d}_{zx}^{(1)}\right) \Big/ \left(1 + (V_3/V_4)^2\right)^{1/2}, \tag{E.12}$$

$$\psi_4^{\pm} = \frac{-\Delta_0 \pm \sqrt{\Delta_0^2 + 8V_1^2}}{4V_1} \frac{1}{\alpha_4^{\pm}} \left({\rm d}_{xy}^{(1)} + {\rm d}_{xy}^{(2)}\right) + \frac{1}{\alpha_4^{\pm}} {\rm p}_x, \tag{E.13}$$

$$\psi_5^{\pm} = \frac{-\Delta_0 \pm \sqrt{\Delta_0^2 + 8V_2^2}}{4V_2} \frac{1}{\alpha_5^{\pm}} \left({\rm d}_{xy}^{(1)} - {\rm d}_{xy}^{(2)}\right) + \frac{1}{\alpha_5^{\pm}} {\rm p}_y, \tag{E.14}$$

$$\begin{aligned} \psi_6^{\pm} = {} & \frac{2}{\Delta_0 \pm \sqrt{\Delta_0^2 + 8(V_3^2 + V_4^2)}} \frac{1}{\alpha_6^{\pm}} \\ & \times \left(V_4 {\rm d}_{yz}^{(1)} + V_3 {\rm d}_{zx}^{(1)} + V_4 {\rm d}_{yz}^{(2)} - V_3 {\rm d}_{zx}^{(2)}\right) + \frac{1}{\alpha_6^{\pm}} {\rm p}_z, \end{aligned} \tag{E.15}$$

where

$$\alpha_4^{\pm} = \sqrt{1 + \frac{1}{8}\left(\frac{-\Delta_0 \pm \sqrt{\Delta_0^2 + 8V_1^2}}{V_1}\right)^2},$$

$$\alpha_5^{\pm} = \sqrt{1 + \frac{1}{8}\left(\frac{-\Delta_0 \pm \sqrt{\Delta_0^2 + 8V_2^2}}{V_2}\right)^2},$$

$$\alpha_6^{\pm} = \sqrt{1 + \frac{8(V_3^2 + V_4^2)}{\left(\Delta_0 \pm \sqrt{\Delta_0^2 + 8(V_3^2 + V_4^2)}\right)^2}}$$

are the normalization factors.

The remaining task is to calculate the polarization $\langle e\mathbf{r}\rangle$ for each of the eigenstates obtained. With the help of two-center dipole integrals in appendix D, the final expression of the electric dipole moment $\mathbf{P}$ for each of the eigenstates above read

$$\begin{aligned} \mathbf{P}_1 &= \langle\psi_1|e\mathbf{r}|\psi_1\rangle = 0 \\ &= \mathbf{P}_2 = \mathbf{P}_3, \end{aligned} \tag{E.16}$$

$$\mathbf{P}_4^{\pm} = \left\langle\psi_4^{\pm}|e\mathbf{r}|\psi_4^{\pm}\right\rangle = \frac{\pm 4V_1}{\sqrt{\Delta_0^2 + 8V_1^2}} I_{xy,x}^{y} \hat{e}_y, \tag{E.17}$$

$$\mathbf{P}_5^{\pm} = \left\langle\psi_5^{\pm}|e\mathbf{r}|\psi_5^{\pm}\right\rangle = \frac{\pm 4V_2}{\sqrt{\Delta_0^2 + 8V_2^2}} I_{xy,y}^{y} \hat{e}_y, \tag{E.18}$$

$$\begin{aligned} \mathbf{P}_6^{\pm} &= \left\langle\psi_6^{\pm}|\mathbf{r}|\psi_6^{\pm}\right\rangle \\ &= \frac{\pm 4}{\sqrt{\Delta_0^2 + 8(V_3^2 + V_4^2)}} \left(V_4 I_{yz,z}^{y} + V_3 I_{zx,z}^{y}\right) \hat{e}_y, \end{aligned} \tag{E.19}$$

where $I_{\mu,\nu}^{y}$ ($\mu = xy, yz, zx$; $\nu = x, y, z$) are the overlap dipole matrix elements as defined in equation (20). Note that nonzero polarization develops solely along the y direction in such a M_1–O–M_2 cluster.

From equations (E.6) to (E.9), we know that the three low-energy states are ε_4^-, ε_5^- and ε_6^-, which vary with the bond-bending angle φ. The corresponding wavefunctions are ψ_4^-, ψ_5^- and ψ_6^-, respectively and their induced electric dipole moments are $\mathbf{P}_4^-$, $\mathbf{P}_5^-$ and $\mathbf{P}_6^-$. If two holes are introduced in the cluster, two of these three states become the ground state depending on the values of bond-bending angle φ. As a representative case, we here simply choose ψ_4^- and ψ_5^- as the ground state and consider the lattice-driven electric dipole moment $\mathbf{P}^{\rm ld} = \mathbf{P}_4^- + \mathbf{P}_5^-$. We show in figure 8(a) the φ-dependence of the polarization $P^{\rm ld}$ ($P^{\rm ld}$ is the electric dipole moment $\mathbf{P}^{\rm ld}$ per unit volume). It should be noted that, we can choose the other two of the three low-energy states as the ground state and find that their $P^{\rm ld}$ show similar

behaviors. In figure 8(a), we choose the parameters: cubic lattice constant $a = 5$ Å, $\Delta_0 = 2$ eV, $t_{pd\sigma}/t_{pd\pi} = -2$, and typical M–O separation $R_{M\text{–}O} = 4a_0$ (a_0 is the Bohr radius). The Clementi–Raimondi effective charges are chosen as $Z_O^{eff} = 4.45$ and $Z_M^{eff} = 10.53$ for O^{2-} and M ions respectively. We also assume that each unit cell contains only one M_1–O–M_2 cluster. It is worth noting that the lattice-driven polarization P^{ld} vanishes if there is no bond-bending.

References

[1] Fiebig M 2005 *J. Phys. D: Appl. Phys.* **38** R123
[2] Hill N A 2000 *J. Phys. Chem.* B **104** 6694
[3] Kimura T, Goto T, Shintani H, Ishizaka K, Arima T and Tokura Y 2003 *Nature* **426** 55
[4] Kenzelmann M, Harris A B, Jonas S, Broholm C, Schefer J, Kim S B, Zhang C L, Cheong S-W, Vajk O P and Lynn J W 2005 *Phys. Rev. Lett.* **95** 087206
[5] Cheong S-W and Mostovoy M 2007 *Nature Mater.* **6** 13
[6] Loidl A, von Loehneysen H and Kalvius G M (ed) 2008 *J. Phys.: Condens. Matter* **20** 430301
[7] Khomskii D 2009 *Physics* **2** 20
[8] Wang K F, Liu J-M and Ren Z F 2009 *Adv. Phys.* **58** 321
[9] Katsura H, Nagaosa N and Balatsky A V 2005 *Phys. Rev. Lett.* **95** 057205
[10] Jia C, Onoda S, Nagaosa N and Han J H 2006 *Phys. Rev.* B **74** 224444
[11] Jia C, Onoda S, Nagaosa N and Han J H 2007 *Phys. Rev.* B **76** 144424
[12] Hu J 2008 *Phys. Rev. Lett.* **100** 077202
[13] Hu C D 2007 *Phys. Rev.* B **75** 172106
[14] Hu C D 2008 *Phys. Rev.* B **77** 174418
[15] Hu C D 2010 *Phys. Rev.* B **81** 224414
[16] Sergienko I A and Dagotto E 2006 *Phys. Rev.* B **73** 094434
[17] Mochizuki M, Furukawa N and Nagaosa N 2010 *Phys. Rev. Lett.* **105** 037205
[18] Mochizuki M, Furukawa N and Nagaosa N 2011 *Phys. Rev.* B **84** 144409
[19] Mostovoy M 2006 *Phys. Rev. Lett.* **96** 067601
[20] Yamasaki Y, Sagayama H, Goto T, Matsuura M, Hirota K, Arima T and Tokura Y 2007 *Phys. Rev. Lett.* **98** 147204
[21] Goto T, Kimura T, Lawes G, Ramirez A P and Tokura Y 2004 *Phys. Rev. Lett.* **92** 257201
[22] Taniguchi K, Abe N, Takenobu T, Iwasa Y and Arima T 2006 *Phys. Rev. Lett.* **97** 097203
[23] Lawes G *et al* 2005 *Phys. Rev. Lett.* **95** 087205
[24] Yamasaki Y, Miyasaka S, Kaneko Y, He J-P, Arima T and Tokura Y 2006 *Phys. Rev. Lett.* **96** 207204
[25] Park S, Choi Y J, Zhang C L and Cheong S-W 2007 *Phys. Rev. Lett.* **98** 057601
[26] Seki S, Yamasaki Y, Soda M, Matsuura M, Hirota K and Tokura Y 2008 *Phys. Rev. Lett.* **100** 127201
[27] Naito Y, Sato K, Yasui Y, Kobayashi Y, Kobayashi Y and Sato M 2007 *J. Phys. Soc. Japan* **76** 023708
[28] Yasui Y, Naito Y, Sato K, Moyoshi T, Sato M and Kakurai K 2008 *J. Phys. Soc. Japan* **77** 023712
[29] Schrettle F, Krohns S, Lunkenheimer P, Hemberger J, Büttgen N, Krug von Nidda H-A, Prokofiev A V and Loidl A 2008 *Phys. Rev.* B **77** 144101
[30] Mourigal M, Enderle M, Kremer R K, Law J M and Fåk B 2011 *Phys. Rev.* B **83** 100409
[31] Xiang H J, Kan E J, Zhang Y, Whangbo M-H and Gong X G 2011 *Phys. Rev. Lett.* **107** 157202
[32] Lu X Z, Whangbo M-H, Dong S, Gong X G and Xiang H J 2012 *Phys. Rev. Lett.* **108** 187204
[33] Yang J H, Li Z L, Lu X Z, Whangbo M-H, Wei S-H, Gong X G and Xiang H J 2012 *Phys. Rev. Lett.* **109** 107203
[34] Li Z-L, Whangbo M-H, Gong X G and Xiang H J 2012 *Phys. Rev.* B **86** 174401
[35] Kimura T, Ishihara S, Shintani H, Arima T, Takahashi K T, Ishizaka K and Tokura Y 2003 *Phys. Rev.* B **68** 060403
[36] Arima T, Tokunaga A, Goto T, Kimura H, Noda Y and Tokura Y 2006 *Phys. Rev. Lett.* **96** 097202
[37] Moskvin A S and Drechsler S-L 2008 *Phys. Rev.* B **78** 024102
[38] Slater J C and Koster G F 1954 *Phys. Rev.* **94** 1498
[39] Landau L D and Lifshitz E M 1991 *Quantum Mechanics* (London: Pergamon) p 138
[40] Mizokawa T and Fujimori A 1995 *Phys. Rev.* B **51** 12880
[41] Capogna L, Mayr M, Horsch P, Raichle M, Kremer R K, Sofin M, Maljuk A, Jansen M and Keimer B 2005 *Phys. Rev.* B **71** 140402
[42] Choi K-Y, Gnezdilov V P, Lemmens P, Capogna L, Johnson M R, Sofin M, Maljuk A, Jansen M and Keimer B 2006 *Phys. Rev.* B **73** 094409
[43] Gippius A A, Moskvin A S and Drechsler S-L 2008 *Phys. Rev.* B **77** 180403
[44] Capogna L, Reehuis M, Maljuk A, Kremer R K, Ouladdiaf B, Jansen M and Keimer B 2010 *Phys. Rev.* B **82** 014407
[45] Leininger Ph *et al* 2010 *Phys. Rev.* B **81** 085111
[46] Xiang H J and Whangbo M-H 2007 *Phys. Rev. Lett.* **99** 257203
[47] Pickett W E 1989 *Rev. Mod. Phys.* **61** 433
[48] Clementi E and Raimondi D L 1963 *J. Chem. Phys.* **38** 2686
[49] Koo H-J, Lee C, Whangbo M-H, McIntyre G J and Kremer R K 2011 *Inorg. Chem.* **50** 3582